Flooding in Western Washington: The Connection to Atmospheric Rivers*

PAUL J. NEIMAN

Physical Sciences Division, NOAA/Earth System Research Laboratory, Boulder, Colorado

LAWRENCE J. SCHICK

U.S. Army Corps of Engineers, Seattle, Washington

F. MARTIN RALPH

Physical Sciences Division, NOAA/Earth System Research Laboratory, Boulder, Colorado

MIMI HUGHES

NOAA/ESRL and Cooperative Institute for Research in the Environmental Sciences, Boulder, Colorado

GARY A. WICK

Physical Sciences Division, NOAA/Earth System Research Laboratory, Boulder, Colorado

(Manuscript received 8 July 2010, in final form 14 April 2011)

ABSTRACT

This study utilizes multiple decades of daily streamflow data gathered in four major watersheds in western Washington to determine the meteorological conditions most likely to cause flooding in those watersheds. Two are located in the Olympic Mountains and the other two in the western Cascades; and each has uniquely different topographic characteristics. The flood analysis is based on the maximum daily flow observed during each water year (WY) at each site [i.e., the annual peak daily flow (APDF)], with an initial emphasis on the 12 most recent water years between WY1998 and 2009, and then focusing on a 30-year interval between WY1980 and 2009. The shorter time period coincides with relatively complete passive microwave satellite coverage of integrated water vapor (IWV) over the Pacific basin. The combination of IWV imagery and streamflow data highlights a close link between landfalling atmospheric rivers (ARs) and APDFs (i.e., 46 of the 48 APDFs occurred with landfalling ARs). To complement this approach, the three-decade time series of APDFs, which correspond to the availability of the North American Regional Reanalysis (NARR) dataset, are examined. The APDFs occur most often, and are typically largest in magnitude, from November to January. The NARR is used to assess the composite meteorological conditions associated with the 10 largest APDFs at each site during this 30-year period. Heavy precipitation fell during the top 10 APDFs, and anomalously high composite NARR melting levels averaged ~1.9 km MSL, which is primarily above the four basins of interest. Hence, on average, mostly rain rather than snow fell within these basins, leading to enhanced runoff. The flooding on the four watersheds shared common meteorological attributes, including the presence of landfalling ARs with anomalous warmth, strong low-level water vapor fluxes, and weak static stability. There were also key differences that modulated the orographic control of precipitation. Notably, two watersheds experienced their top 10 APDFs when the low-level flow was southwesterly, while the other two basins had their largest APDFs with west–southwesterly flow. These differences arose because of the region's complex topography, basin orientations, and related rain shadowing.

* Supplemental information related to this paper is available at the Journals Online Web site: http://dx.doi.org/10.1175/2011JHM1358.s1.

Corresponding author address: Paul J. Neiman, NOAA/ESRL/Physical Sciences Division, 325 Broadway, Boulder, CO 80305.
E-mail: Paul.J.Neiman@noaa.gov

DOI: 10.1175/2011JHM1358.1

1. Introduction

The climate of western Washington is temperate maritime, characterized by wet winters with little or no lowland snow and relatively dry summers. The heavy precipitation and flood season is focused from late October to mid-March. Annual precipitation in western Washington varies considerably, from about 950 mm in Seattle to as little as ~375 mm in the ''rain-shadowed'' town of Sequim to 2000–5000 mm in the nearby Olympic and Cascade Mountains (Fig. 1). The precipitation distribution is modulated to first order by orographic forcing, as moisture-laden, landfalling Pacific storms encounter the region's steep terrain (e.g., Colle et al. 2000; Minder et al. 2008). Given the combination of rugged topography and heavy cool-season rains, the river basins here are prone to quick runoff typically evolving on time scales of a few hours to roughly two days. Despite the abundant snowpack at higher elevations, western Washington does not often experience spring-melt flooding, as river basin channel capacity is considerable and has evolved to accommodate heavy runoff volume from copious winter rainfall.

Landfalling extratropical cyclones along the U.S. West Coast typically contain enhanced onshore water vapor fluxes in the warm sector, especially during the baroclinically active cool season. A subset of those storms that tap into the tropical water vapor reservoir and/or are accompanied by strongly confluent flow ahead of the polar cold front concentrate those fluxes into long (>~2000 km), narrow (<~1000 km) plumes (e.g., Bao et al. 2006; Stohl et al. 2008; Ralph et al. 2011). These plumes, referred to as atmospheric rivers (ARs), are situated in the lower troposphere within a broader region of generally poleward heat transport in the warm sector (e.g., Zhu and Newell 1998; Ralph et al. 2004; Neiman et al. 2008a,b). ARs are characterized by moist-neutral stratification offshore (Ralph et al. 2005) and, thus, when combined with their often strong low-level flow and large water vapor content, are predisposed to significant orographic precipitation enhancement upon landfall. Precipitation can be enhanced further if an AR moves slowly or stalls over a given region (e.g., Ralph et al. 2011). Recent climatological studies along the U.S. West Coast have shown that landfalling winter storms with AR attributes produce twice as much precipitation as non-AR storms (Neiman et al. 2008b) and, in California's Sierra Nevada, yield daily increases in streamflow that are an order of magnitude larger than those from non-AR storms (Dettinger 2004). ARs are responsible for >90% of the horizontal water vapor transport in less than 10% of the zonal circumference at midlatitudes (Zhu and Newell 1998) and, thus, play a role in the global water cycle.

A particularly intense AR impacted the Pacific Northwest on 6–7 November 2006 (Fig. 2; from Neiman et al. 2008a). Satellite imagery constructed from data recorded by Special Sensor Microwave Imagers (SSM/I; Hollinger et al. 1990) (Fig. 2a) shows a narrow AR with enhanced integrated water vapor (IWV) extending northeastward from the tropical eastern Pacific to western Washington. Rainfall in the Cascades and coastal mountains ranged from 250 to 750 mm (Fig. 2c). The melting-level altitude for this case (>3 km MSL; not shown) was ~1.2 km above (i.e., 135–150 hPa less than) the climatological mean (Fig. 2b). These remarkably high melting levels resulted in rain falling at high elevations over a much larger catchment area for runoff than during a typical storm, thus leading to greatly enhanced runoff volume (e.g., White et al. 2002; Lundquist et al. 2008). In response to the heavy rainfall and high melting levels, most of the streams draining the coastal mountains and Cascades yielded maximum 1-day flows among the top 1% of those observed historically for November, with six gauges recording all-time record November flows (Fig. 2d). Three years earlier, another intense AR impacted Washington in late October 2003, resulting in rapid filling of, and subsequent large releases from, area reservoirs, despite the fact that this storm was the first of the rainy season with no preexisting snowpack, and it immediately followed a record dry summer. During that AR, Seattle broke its all-time 24-h rainfall total of 128 mm on 20 October, shattering the previous record of 87 mm on 29 November 1959. A similar connection between landfalling ARs and flooding has been documented in California (e.g., Dettinger 2004; Ralph et al. 2006) and in western Europe (Stohl et al. 2008). Likewise, Lackmann and Gyakum (1999) tied a flood event in western Washington to the

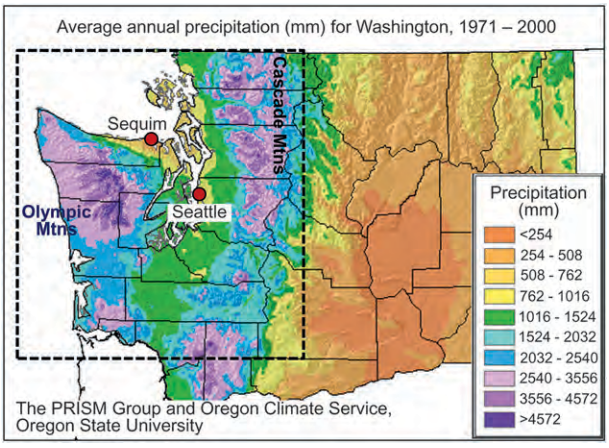

FIG. 1. Average annual precipitation (mm; see color key) for Washington from 1971 to 2000, using the Parameter-elevation Regressions on Independent Slopes Model (PRISM; Daly et al. 1994). The dashed inset box is the domain shown in Fig. 3. The analysis is from the PRISM group and Oregon Climate Service, Oregon State University.

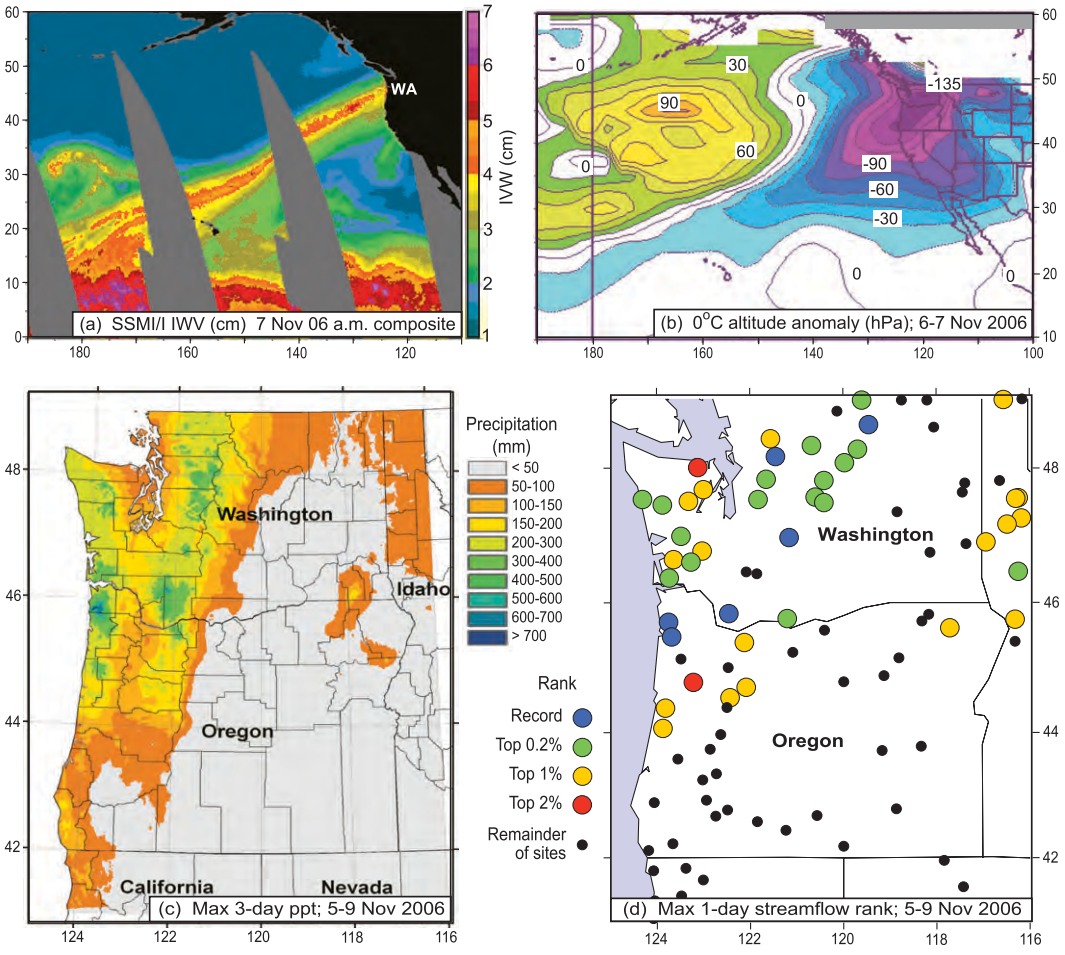

FIG. 2. Summary conditions of the AR that devastated the Pacific Northwest in early November 2006 (as in Neiman et al. 2008a): (a) composite SSM/I satellite image of IWV (cm) between 0000 and 1200 UTC 7 Nov 2006 (derived using the algorithm of Schluessel and Emery 1990), (b) NCAR–NCEP global reanalysis (Kalnay et al. 1996) of the 0°C altitude anomaly (hPa) for 6–7 Nov 2006 (relative to the 30-year mean between 1968 and 1996), (c) greatest three-day precipitation totals (mm) between 5 and 9 Nov 2006; and (d) maximum ranking between 5 and 9 Nov 2006 of daily unregulated streamflows during the month of November for those gauges that have recorded data for at least 30 Novembers.

landfall of a winter storm with AR attributes. Finally, Knippertz and Wernli (2010) highlighted the climatological importance of ARs of tropical and/or subtropical origin (which they refer to as "tropical moisture exports") to West Coast precipitation.

During major floods in western Washington, the U.S. Army Corps of Engineers' Reservoir Control Center (RCC) in Seattle utilizes hydrologic forecasts from the National Oceanic and Atmospheric Administration's (NOAA) Northwest River Forecast Center to direct dam operations for managing downstream flood risk, including at the Howard Hanson Dam on the Green River, the Wynoochee Dam on the Wynoochee River, and the Ross and Upper Baker Dams in the Skagit River basin. The RCC coordinates with Corps Emergency Management and local, county, state, and federal agencies to manage flood risk reduction activities. The strategy is to evaluate changing weather and hydrologic forecasts while using reservoir storage, basin characteristics, known levee limitations, and other factors to manage the flood risk, with the acknowledgment that, downstream from reservoirs in western Washington, low-elevation tributaries can contribute runoff greater than 50% of the total flow beyond the management of the dams. The approach is to capture and store the peak of the flood waters behind the dams until the threat passes. Then, immediately after the event, release as much water as is prudent, to make storage available for a possible subsequent rain event.

The area in western Washington with the greatest potential flood-related consequences resides downstream of the Howard Hanson Dam on the Green River. The Green meanders through the populated Kent Valley,

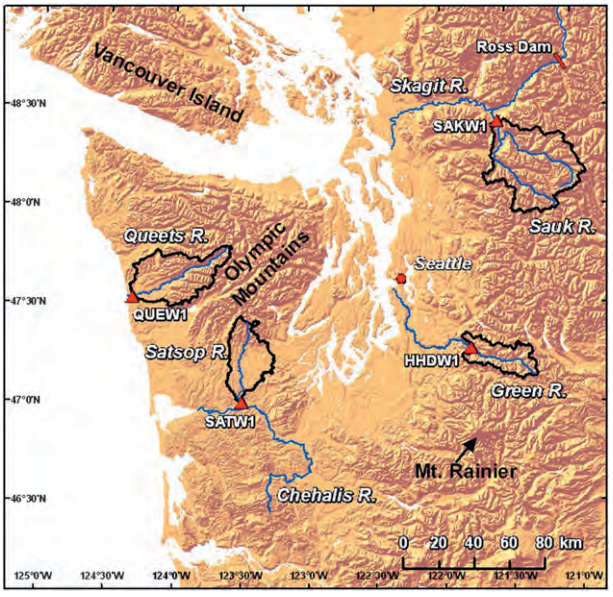

FIG. 3. Terrain base map of western Washington showing the locations of the four rivers (blue), basin areas (outlined in black), and stream gauges (red triangles) (HHDW1, SAKW1, SATW1, and QUEW1) that are discussed in this study. The locations of Ross Dam and Seattle are also shown.

south of Seattle. The dam and downstream levees assist in flood-risk management of many billions of dollars in infrastructure and the protection of tens of thousands of people. The Kent Valley is considered the second largest industrial warehouse district on the West Coast of the United States and is home to a major Boeing defense facility. During a major AR event in January 2009 (Mastin et al. 2010), floodwaters were stored behind Howard Hanson Dam. The resulting record-high reservoir level behind the dam focused attention on seepage issues through the dam's right abutment—a 10 000-year-old landslide hillside. This raised concerns regarding future flood storage capacity. Hence, until the seepage issue is adequately mitigated, confidence in the dam's full water storage capacity is reduced.

In the above context, key questions arise: although landfalling ARs produce floods, are most floods the result of ARs, and, if so, what is the percentage? This study will attempt to answer these questions by analyzing a multidecade record of streamflow data from four major watersheds in western Washington, as well as using mesoscale reanalysis data for the same 30 years and SSM/I satellite observations during a shorter 12-yr time period.

2. Data sources

This study utilizes streamflow data gathered in four major river basins across western Washington. The measurement sites were chosen because the selected basins cover a wide geographic area, have long records of unregulated streamflows, and reflect the variability of terrain and orientation that exist in the region (Fig. 3 and Table 1; discussed in more detail in section 3). Two of the gauge sites are located in the Olympic Mountains and both are operated by the U.S. Geological Survey (USGS): the Queets River near Clearwater (QUEW1) and the Satsop River near Satsop (SATW1). These rivers drain the western and southern flanks of the Olympics, respectively. Two additional measurement sites along the western slope of the Cascades include the Sauk River near Sauk (SAKW1) and the Green River at Howard Hanson Dam (HHDW1). The Sauk gauge resides in the Skagit River basin and is operated by the USGS. Farther south, the Army Corps monitors the Green River inflows into the reservoir behind Howard Hanson Dam. The inflows are calculated by knowing the discharge volume from the dam and the change of volume of the reservoir. Streamflow records extend back 48 yr at HHDW1 (i.e., since the commissioning of the dam), with much longer records of 80–82 yr at the three other sites, although this study will focus on data taken during the most recent 30 water years[1] (WY) from WY1980 to 2009. The four measurement sites obtain instantaneous flows, from which mean daily values are calculated. Although the instantaneous flows give a truer measure of the maximum discharge during an individual flood event, the daily data provide more information on the total volume of an event, which is more relevant to water resource management, including flood-risk management activities.

The IWV data used in this study were collected from SSM/I and Special Sensor Microwave Imager/Sounder (SSMIS) observing platforms aboard polar orbiting satellites that circled the globe every ~102 min. SSM/I IWV data from the *F13* satellite were available between 1 October 1997 and 30 September 2009 (i.e., WY1998–2009), while the *F11*, *F14*, and *F15* satellites provided additional SSM/I IWV data between 1 October 1997 and 17 May 2000, 1 October 1997 and 24 August 2008, and 23 February 2000 and 14 September 2006, respectively. The *F16* and *F17* satellites provided supplemental SSMIS IWV data between 1 October 2008 and 30 September 2009. The IWV was retrieved using primarily the Schluessel and Emery (1990) algorithm. This algorithm uses three channels from SSM/I including the 85.5 GHz vertically polarized channel. For SSMIS, the frequency of the channel closest to 85.5 GHz was changed to 91.655 GHz. To

[1] A water year is shifted three months earlier than a calendar year, beginning on 1 Oct and ending on 30 Sep. For example, water year 1998 starts on 1 Oct 1997 and ends on 30 Sep 1998.

TABLE 1. Stream gauge and upstream watershed information for four locations in western Washington.

River basin	Gauge location	Gauge name	Gauge latitude (°N)	Gauge longitude (°W)	Gauge elevation (m)	Basin area above gauge (km^2)	Years available
Green	Hanson Dam inflow*	HHDW1	47.283	121.783	368	572	48
Sauk	Near Sauk	SAKW1	48.425	121.567	81	1848	82
Satsop	Near Satsop	SATW1	47.000	123.494	6	774	81
Queets	Near Clearwater	QUEW1	47.538	124.314	4	1152	80

* The inflow values at Hanson Dam are calculated based on the dam discharge volume and change in volume of the reservoir rather than being measured directly by a gauge.

avoid potential issues related to this change in frequency, the Wentz (1995) optimal statistical algorithm was used for the period incorporating SSMIS. This algorithm uses only the 19.35 and 22.235 GHz vertically polarized channels, which remained similar for SSM/I and SSMIS. These data, which have a native resolution of ~40 km in ~1400-km-wide swaths, were placed on a ~25-km-resolution grid and combined into twice-daily composite images corresponding to the time intervals between 0000 and 1159 UTC and 1200 and 2359 UTC. Prior to WY1998, fewer satellites were available and yielded comparatively poorer satellite coverage, so these earlier years were not included in the IWV data analysis.

The North American Regional Reanalysis (NARR; Mesinger et al. 2006) database was used to assess the meteorological conditions responsible for flooding at the four stream measurement sites. Covering all of North America and adjacent oceans, the NARR is available from 1979 to present with a horizontal grid spacing of 32 km and 45 vertical levels. The reanalysis blends observational and model first-guess data to estimate the state of the atmosphere at 3-h intervals. It ingests initial conditions from the operational Eta Data Assimilation System (Rogers 2005) and assimilates precipitation observations using derived latent heating profiles. Studies by Bukovsky and Karoly (2007) and Becker et al. (2009) show that the NARR provides a reasonable first-order estimate of the large-scale cool-season U.S. precipitation, although its coarse 32-km resolution relative to the finescale topography of the western United States clearly limits its ability to accurately depict basin-scale orographic precipitation modulation. A paper by West et al. (2007) cautions against spurious gridscale precipitation in the NARR, although the results presented later show no evidence of such artifacts. Mo et al. (2005) demonstrate that NARR's precipitation and moisture transports are most realistic during winter, which corresponds approximately to our cool-season focus. Finally, a study by Ruane (2010) shows weaknesses with the NARR water cycle over the northeastern Pacific. However, given that our study uses NARR precipitation in a qualitative large-scale context only, the issues described above should not adversely impact the veracity of our key findings.

3. River basin and streamflow characteristics

The three USGS stream gauge sites used in this study (i.e., SAKW1, SATW1, and QUEW1) are all located at low elevation between 4 and 81 m MSL, while the Army Corps site at HHDW1 resides at 368 m MSL (Table 1). The basin areas above these sites vary by a factor of ~3.2 (i.e., from 1848 to 572 km^2), with the Sauk possessing the largest area, followed by the Queets, the Satsop, and then the Green. Unquestionably, the basin with the greatest direct exposure to the Pacific is the west–southwest-oriented Queets, which drains a sizeable portion of the western flank of the Olympic Mountains (Fig. 3). Portions of the Queets basin contain the wettest climate in the contiguous United States, receiving as much as 5000 mm of precipitation annually (Fig. 1). The nearby Satsop drains part of the Olympics' southern slopes and flows into the mainstream Chehalis River, but it is partially protected from landfalling storms by the higher terrain of this range to the west. The Sauk, located in the north Cascades, is the southernmost tributary in the Skagit River basin. The Sauk contributes roughly half of the unregulated flow to the Skagit, which is the largest river system in western Washington and one of the largest on the West Coast of the contiguous United States. The Skagit is oriented generally west–east, while the Sauk tributary faces northwestward. Given that this entire region resides east of the Olympics and adjacent mountains of Vancouver Island, direct low-level airflow from the Pacific occurs only from the southwest quadrant. Finally, the west–east-oriented Green River is located farther south in the Cascades, east–southeast of the Olympics and due north of the Mt. Rainier massif. Because of the proximity of these formidable mountains to the Green, direct low-level flow from the Pacific occurs only in a narrow wind-direction window from ~245° to 275°.

It is important to consider not only the basin area and orientation above each stream gauge, but also the basin's

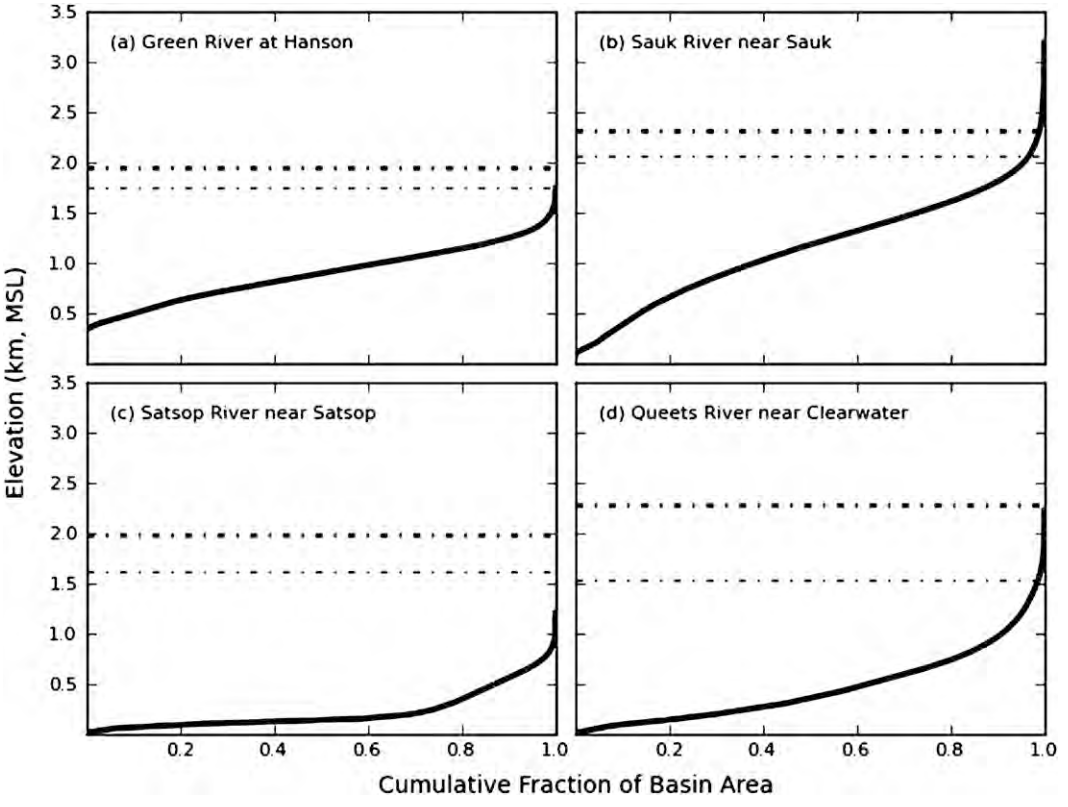

FIG. 4. Cumulative fraction of basin area as a function of basin elevation upstream of the following four sites: (a) HHDW1, (b) SAKW1, (c) SATW1, and (d) QUEW1. The thick (thin) horizontal line in each panel marks the NARR-estimated composite melting-level altitude based on the day of (day before) the top 10 annual peak daily flows for that site.

elevation characteristics. Specifically, the relationship between the elevation and fractional area of a basin dictates the amount of rain versus snow that falls within the drainage domain for a given melting-level altitude (i.e., the altitude at which snow melts to rain), which, in turn, critically impacts the magnitude of runoff. Figure 4 depicts the cumulative fraction of basin area as a function of elevation upstream of each of the four gauges. The Green is a low- to middle-elevation basin whose headwaters reach upward to ~1.75 km MSL along the windward slope of Washington's central Cascades (Fig. 4a). Roughly two-thirds of the basin sits between 0.7 and 1.3 km MSL and three-quarters is below ~1.2 km MSL In contrast, the Sauk drains much higher terrain in the north Cascades, including 3213-m Glacier Peak, with two-thirds of that basin nestled between ~0.7 and 1.8 km MSL and three-quarters below 1.6 km MSL (Fig. 4b). The Satsop, in the southern Olympics, is the lowest of the four basins, draining topography that extends up to only 1.25 km MSL (Fig. 4c). Fully three-quarters of the basin sits below 250 m MSL and, hence, receives almost entirely rain. Finally, the Queets penetrates deep into the upper reaches of the Olympics, including the south flank of 2432-m Mt. Olympus (Fig. 4d). Nevertheless, only ~20% of the Queets basin extends above 750 m MSL, so it, too, receives a large proportion of rain (rather than snow). The vegetation in the Sauk, Green, and Satsop basins are mainly coniferous second growth forests, often with deciduous trees in the riparian sections, as well as areas of clear cut. The Queets is one of the most pristine river basins in the lower 48 states, with substantial old growth forest. It is located primarily in the protected Olympic National Park. The soils in the four basins range from excessively to moderately well drained on steep slopes to floodplains, and they are formed largely of river wash to deep silt loams.

In an effort to assess the rarity of flow magnitudes at each of the four gauges, a flood frequency analysis was carried out based on the methodology described in USGS (1981). This analysis incorporates the maximum daily flow observed during each water year [referred to as the annual peak daily flow (APDF)] of the complete multidecadal time series at each site. The resulting site-dependent curves in Fig. 5 show the return period or

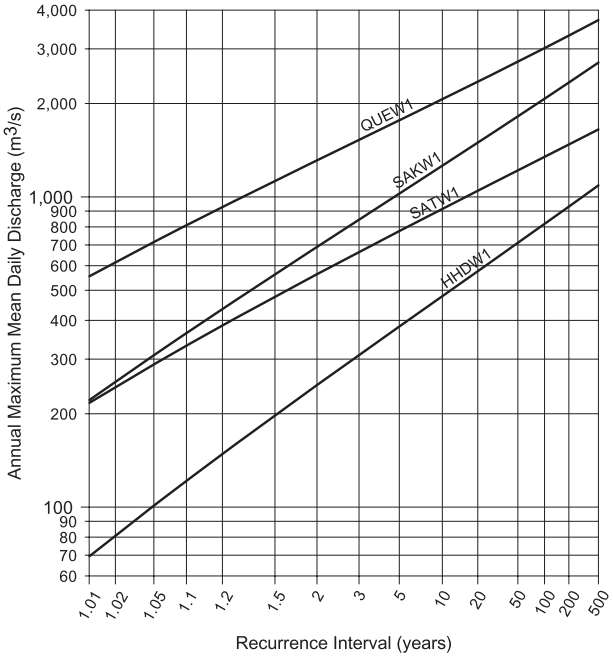

FIG. 5. Return period (yr) of annual peak daily flows ($m^3 s^{-1}$) at HHDW1, SAKW1, SATW1, and QUEW1.

recurrence interval in years based on the APDFs. The magnitude of the streamflows for a given return period scales to the basin area, except for the exceptionally large discharges from the Queets due to that basin's direct west-facing exposure to the Pacific. For context, the 5-, 10-, 20-, 50-, and 100-yr return periods are shown in Figs. 6 and 7 in the next section. Although return-period analyses have been employed ubiquitously in the meteorological and hydrological sciences throughout the years, such an approach assumes climatological stationarity—a condition that, at some locales, may no longer be a certainty given global climate change (Milly et al. 2008).

4. Analysis of annual peak daily flows

In this section we present an analysis of APDFs from the four sites, initially emphasizing the 12 most recent water years between WY1998 and 2009 and then focusing on a longer 30-yr interval between WY1980 and 2009. The shorter time period coincides with relatively complete 12-hourly composite microwave satellite coverage of IWV over the Pacific basin. The combination of IWV imagery and streamflow data provides the opportunity to link APDFs to observed AR conditions. To complement this approach, the three-decade time series of APDFs, which correspond to the availability of the NARR dataset, are examined. The NARR will be used to assess the composite meteorological conditions

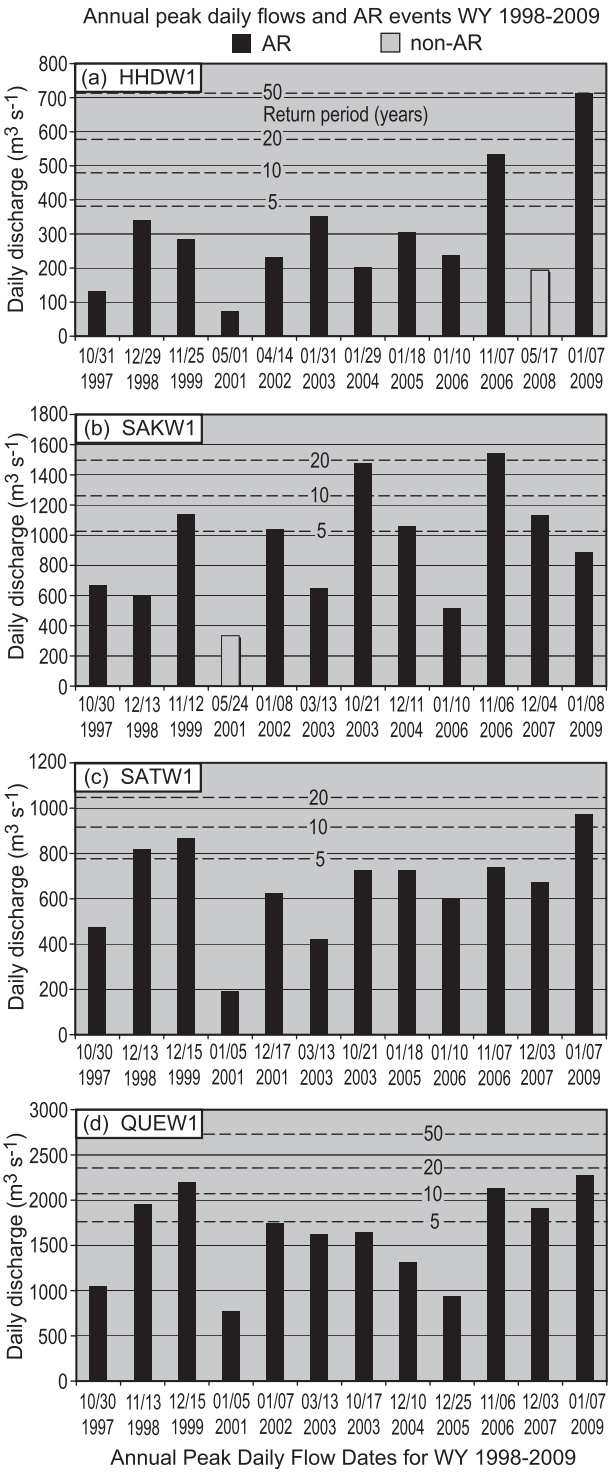

FIG. 6. Interannual distribution of annual peak daily flows ($m^3 s^{-1}$) for WY1998–2009 at (a) HHDW1, (b) SAKW1, (c) SATW1, and (d) QUEW1. Each observed flow is tied to either AR or non-AR conditions (see key) based on SSM/I satellite imagery. Return periods for 5-, 10-, 20-, and 50-yr flows are depicted with horizontal dashed lines. Date format is MM/DD, where MM = month and DD = day.

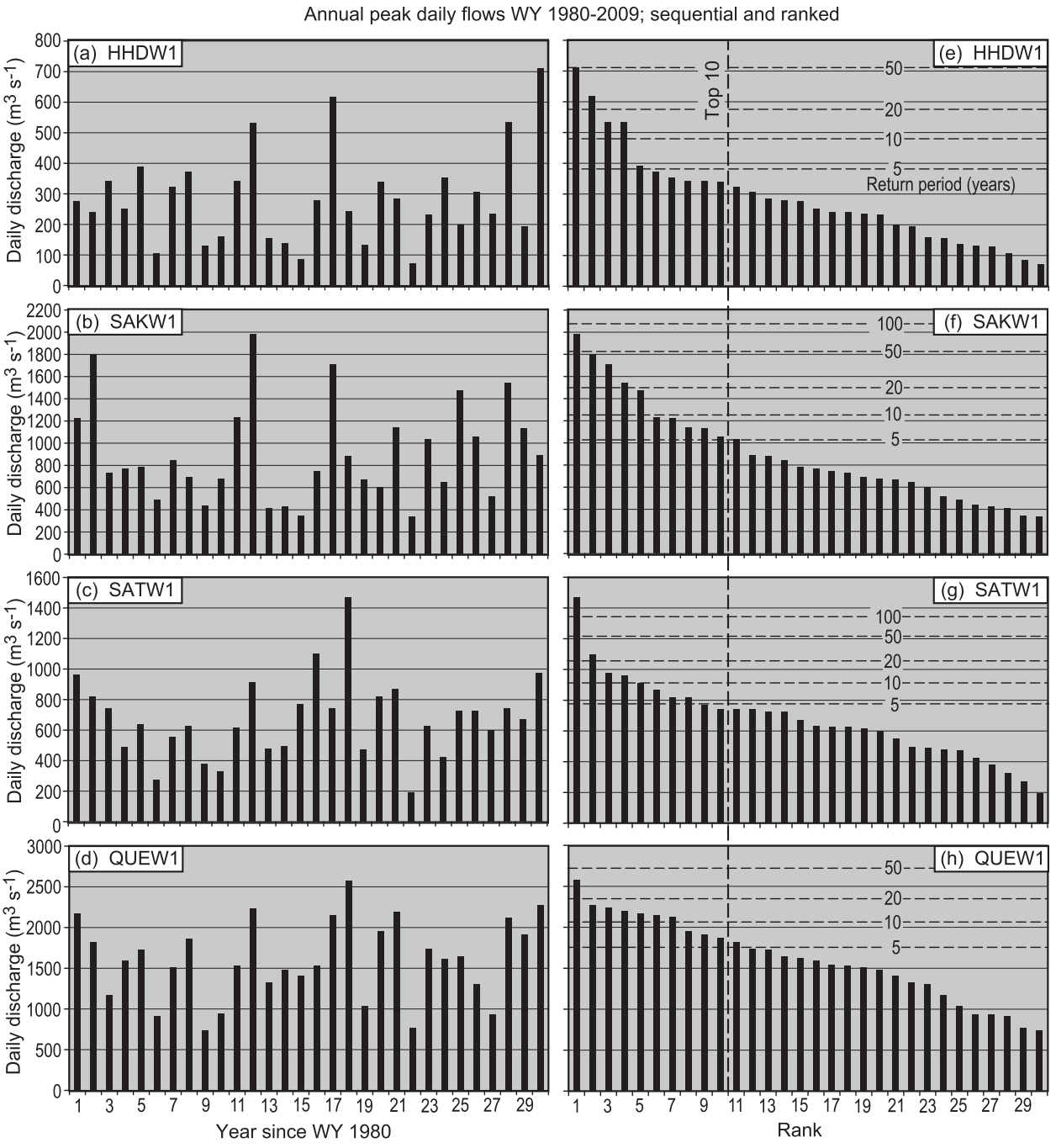

FIG. 7. (a)–(d) Interannual distribution of annual peak daily flows (m^3 s^{-1}) for WY1980–2009 (i.e., years 1 through 30) at (a) HHDW1, (b) SAKW1, (c) SATW1, and (d) QUEW1. (e)–(h) The same data as in (a)–(d), respectively, but ranked from largest to smallest flows. The top 10 ranked flows in (e)–(h) reside to the left of the vertical dashed line, and the return periods for 5-, 10-, 20-, 50-, and 100-year flows are depicted in these panels with horizontal dashed lines.

associated with the 10 largest APDFs at each site during the 30-year period. The rationale for using APDFs rather than peak daily flows exceeding a hydrologically significant threshold is discussed in section 4b in the context of NARR compositing.

a. Twelve water years of records corresponding to available SSM/I satellite observations

To identify possible linkages between APDFs and landfalling ARs, we utilize a variant of a catalog that lists

the dates of all ARs making landfall in western North America between 41.0° and 52.5°N during WY1998–2005. The methodology for creating the original catalog was employed by Neiman et al. (2008b). Using their approach, if a long, narrow plume (>2000 km in length and <1000 km in width) of SSM/I-derived IWV exceeded 2 cm while making landfall in the specified domain during the morning and afternoon SSM/I composite images for a given day, then that day was included in the catalog. In the present study, we employ a less restrictive approach, whereby the date of an AR is included in the revised catalog (not shown) if the landfall occurred between 41.0° and 52.5°N during either the morning or afternoon composite SSM/I IWV imagery on that date. Also, the catalogue published in Neiman et al. (2008b) was extended through WY2009, thereby increasing the sampling period from 8 to 12 yr.

Figure 6 shows distributions of the APDFs at the four measurement sites during the most recent 12 water years. Given that it takes a finite amount of time for rainfall to drain from a basin, an APDF was designated an AR day if an AR made landfall on the day of, or the day before, the APDF. Of the 48 APFDs, 46 were associated with landfalling ARs, thus highlighting the connection between ARs and the largest basin discharges in key watersheds of western Washington. One-third of the AR-related APDFs exceeded a return period of 5 yr, and eight of those flows ranged in magnitude between 10- and 50-yr events. During the 12 water years considered, the largest APDF on the Green, Satsop, and Queets (712, 974, and 2274 $m^3 s^{-1}$, respectively) occurred with the AR of 7–8 January 2009 (Mastin et al. 2010). That storm produced heavy rainfall (rather than snow) within the entirety of those basins. Howard Hanson Dam stored a record-high flood pool arising from the storm's large inflows (~50-yr return period) and flood-risk management operations, during which time a seepage issue was discovered, as described previously. Only one other time since the commissioning of the dam in 1963 did an APDF exceed the 7 January 2009 value: 792 $m^3 s^{-1}$ on 2 December 1977. On the Sauk, the largest APDF between WY1998 and 2009 (i.e., 1540 $m^3 s^{-1}$) occurred during the devastating AR of 6–7 November 2006 (described in detail in Neiman et al. 2008a), when flooding and debris flows ravaged the region, especially along the flanks of Mt. Rainier in Washington and Mt. Hood in Oregon.

The APDFs on the Green and the Sauk not associated with ARs were among the weakest at those sites, and both occurred with enhanced spring snowmelt coinciding with abnormally warm conditions during the latter half of May. The 17 May 2008 snowmelt event on the Green followed a winter with near-normal precipitation falling primarily during abnormally cold conditions (not shown), resulting in few cool-season rain events across the entire Green basin but an unusually deep snowpack at very low altitudes. The region's first significant warm period in mid-May, with freezing levels approaching 4.5 km MSL, rapidly melted the anomalously deep snowpack at lower elevations, thus yielding the largest peak daily flow of the water year. During the 2001 cool season, western Washington experienced very dry conditions (as little as ~50% of normal precipitation in the north Cascades) with no major storms and low streamflows all winter. Hence, the warm episode in late May of that year, with freezing levels of 3.5–4.0 km MSL, rapidly melted the modest snowpack and produced the Sauk's largest daily flow of the season on 24 May.

b. *Thirty water years of records corresponding to the NARR dataset*

In this subsection, we examine a longer 30-yr record of streamflow data at the four sites during the period WY1980–2009, which coincides with the duration of the NARR dataset. Figures 7a–d show the chronological APDFs for this three-decade period. Each site exhibits considerable interannual variability, although the Queets generates the most consistent year-to-year peak flows of the four sites (i.e., varying by a factor of 3.5) while the Green displays the greatest fluctuations (varying by an order of magnitude). The especially large variability on the Green quite likely reflects the narrow range of low-level, onshore wind directions that can reach the basin unobstructed by the complex terrain. The 30 years of APDFs are also presented in ranked order (Figs. 7e–h) so that the NARR can be used to assess the composite meteorological conditions associated with the ten largest APDFs at each site (see section 5). Table 2 lists the dates and magnitudes of these top 10 APDFs. All top 10 APDFs exceed 5-yr flow thresholds, except for five annual measurements on the Green and two on the Satsop. The magnitude of the highest ranked APDF ranges from a ~40-yr event on the Queets to a >100-yr episode on the Satsop.

An alternate approach to assess the composite meteorological conditions associated with large streamflows is to utilize APDF dates in conjunction with dates of peak daily flows surpassing a hydrologically significant threshold, independent of the years they occurred. We employed a daily flow threshold with a 5-yr return period (a conservative threshold for flooding) in an effort to include more cases in the compositing. In doing so, the top 10 APDF dates (Table 2) used to generate NARR composite analyses for the Green, Sauk, Satsop, and Queets increased by only 1, 3, 1, and 4, respectively (not shown). The NARR composites presented in the following section, based on the top 10 APDF dates, did

TABLE 2. Top 10 annual peak daily flows at stream gauges on the Green, Sauk, Satsop, and Queets Rivers in western Washington from WY1980 to 2009.

	Green at Hanson		Sauk near Sauk		Satsop near Satsop		Queets near Clearwater	
Rank	Date	Flow (m^3 s^{-1})	Date	Flow (m^3 s^{-1})	Date	Flow (m^3 s^{-1})	Date	Flow (m^3 s^{-1})
1	7 Jan 2009	712	24 Nov 1990	1 979	19 Mar 1997	1 467	19 Mar 1997	2 580
2	8 Feb 1996	618	26 Dec 1980	1 798	20 Dec 1994	1 099	7 Jan 2009	2 274
3	7 Nov 2006	535	29 Nov 1995	1 710	7 Jan 2009	974	10 Nov 1990	2 240
4	24 Nov 1990	533	6 Nov 2006	1 540	18 Dec 1979	960	15 Dec 1999	2 195
5	25 Jan 1984	391	21 Oct 2003	1 475	24 Nov 1990	912	14 Dec 1979	2 172
6	24 Nov 1986	372	4 Dec 1989	1 229	15 Dec 1999	869	29 Nov 1995	2 149
7	31 Jan 2003	353	18 Dec 1979	1 223	16 Feb 1981	818	6 Nov 2006	2 127
8	24 Jan 1982	343	12 Nov 1999	1 141	13 Dec 1998	818	13 Nov 1998	1 957
9	9 Jan 1990	342	4 Dec 2007	1 133	10 Dec 1993	770	3 Dec 2007	1 911
10	29 Dec 1998	339	11 Dec 2004	1 059	29 Nov 1995	742	23 Nov 1986	1 869

not change meaningfully when the additional peak daily flow cases were included (not shown). By utilizing only the APDF dates in the composites, it is far less likely that any two events in the 30-yr time series were affected by the same combined phases of slow time-scale phenomena [e.g., Madden–Julian oscillation (Madden and Julian 1994), El Niño–Southern Oscillation (Allan et al. 1996), and Pacific decadal oscillation (Mantua et al. 1997)], thus maximizing the probability of case-to-case independence (although several events would be excluded from the compositing).

The streamflow data provide the opportunity to quantify the intra-annual variability of flow magnitudes and frequencies. Figure 8 shows the monthly averaged magnitudes and monthly occurrences of APDFs at the four sites. The greatest number of APDFs arose during the first part of winter (i.e., November–January) when the climatological baroclinic storm track favors the Pacific Northwest; later in winter, the storm track shifts southward to California. The largest monthly averaged APDFs occurred during November on the Green, Sauk, and Queets, which coincides with early season baroclinic storms developing over relatively warm sea surface temperatures that may result in ARs with enhanced water vapor content, heavy rain, and high melting levels (Neiman et al. 2008a). The largest monthly averaged APDF on the Satsop occurred in March, but this finding was biased heavily by the exceptional >100-yr flood event of 1467 m^3 s^{-1} on 19 March 1997. Excluding the March 1997 event, December then produced the greatest monthly averaged APDF on the Satsop, which is still considered early winter.

5. Composite NARR analyses based on top 10 annual peak daily flows

The NARR is used to assess the composite meteorological conditions responsible for the 10 largest APDFs at each of the four sites during the 30-yr period WY1980–2009 (see Figs. 7e–h and Table 2) and to determine if the top 10 peak flows in these basins are associated with uniquely different meteorological attributes. Plan-view composite analyses provide a large-domain perspective, while composite profiles near the Washington coast highlight local meteorological conditions that might play a role in orographic precipitation enhancement.

a. Plan-view composite analyses

To obtain a qualitative first-order estimate of the mean precipitation that fell statewide during the top 10 APDFs, composite two-day NARR precipitation analyses were constructed using the day of, and the day before, those APDFs (Fig. 9). These analyses are examined with the understanding that multiple factors (e.g., duration of precipitation within the 2-day period, areal coverage of stratiform versus convective precipitation, basin elevation characteristics, spatial and temporal snow-level behavior, snowpack, soil composition, and soil moisture) modulate runoff, and, as a result, a 1:1 correspondence between precipitation amount and runoff should not be expected. For the top 10 flows on the Green and Sauk, two-day precipitation totals in the Cascades ranged between ~85 and 150 mm (Figs. 9a,b). For the top 10 flows on the Satsop and Queets, even larger two-day totals of ~100–175 mm fell in the nearby Olympics (Figs. 9c,d).

The composite melting levels from the NARR (which were estimated by subtracting 300 m from the NARR 0°C altitudes, based on observations that the melting level is located ~200–400 m below the 0°C isotherm; e.g., Stewart et al. 1984; White et al. 2002) resided at ~1.5–2.3 km MSL—primarily above the four basins of interest during the two-day precipitation windows (Fig. 4). These melting levels were also well above the climatological value of ~0.95 km MSL, based on 28 yr of in-storm rawinsonde data from Quillayute, Washington (Minder 2010), with the understanding that the NARR

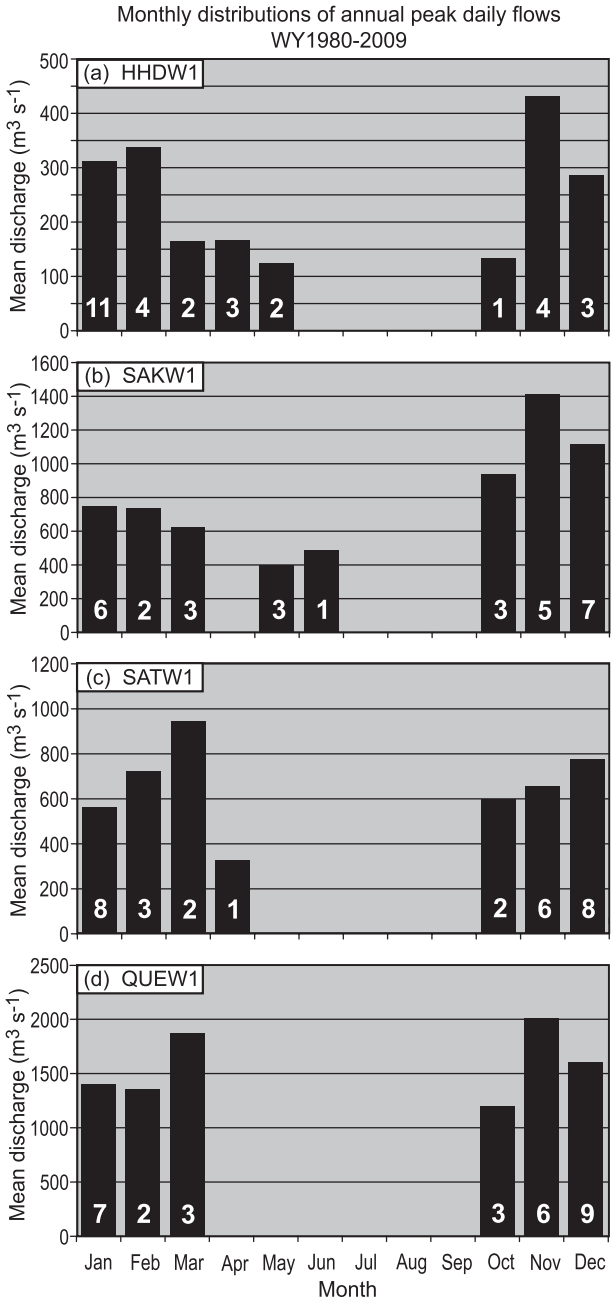

FIG. 8. Monthly averaged distribution of annual peak daily flows ($m^3\ s^{-1}$) for WY1980–2009 at (a) HHDW1, (b) SAKW1, (c) SATW1, and (d) QUEW1. The numbers in the histogram bars denote the monthly occurrences of annual peak daily flow for each month.

might have difficulty capturing the westward extrusion of cold, shallow continental air over the Cascade passes that can locally lower melting levels near these passes (e.g., Steenburgh et al. 1997). Hence, on average, rain rather than snow fell within almost the entirety of these basins, largely because lower-tropospheric temperatures were above normal (described in the following paragraphs). The fact that the melting level above each site ascended between the day-before and day-of NARR composites (day −1 and day 0, respectively) indicates the presence of warm advection and implies synoptic-scale lift (confirmed by NARR omega fields—not shown).

A set of larger-domain NARR composite plan-view analyses, which include 500- and 925-hPa geopotential heights, 925 hPa temperatures, IWV, and vertically integrated horizontal water vapor transport (IVT) between the surface and 300 hPa (Neiman et al. 2008b), are presented for the top 10 APDFs at each of the four stream gauge sites at day −1 and day 0 (Figs. 10–13). Those composites based on the Green River measurements are shown in Fig. 10. The geopotential fields at 500 hPa (Figs. 10a,f) portray a prominent ridge anchored over California and a progressive but weakening trough approaching the Pacific Northwest in west–southwesterly flow. The lower-tropospheric height analyses at 925 hPa (Figs. 10b,g) depict a weakening cyclone over the Gulf of Alaska between day −1 and day 0 and a strong fetch of nearly zonal onshore flow impacting Washington on those two days. Companion temperature analyses at 925 hPa (Figs. 10c,h) capture a well-defined polar baroclinic zone extending offshore from the Washington coast, and companion temperature anomaly analyses (not shown) reveal lower-tropospheric temperatures 4°–6°C above normal over Washington. The baroclinic zone and its frontal circulation, coupled with the approaching shortwave trough aloft, produced large-scale ascent (documented by the NARR—not shown) that contributed to widespread precipitation. During this 2-day composite period, warm advection increased the height of the melting level by 200 m over HHDW1 (Fig. 4a) and quite likely contributed to the synoptic ascent. The IWV analyses (Figs. 10d,i) show a well-defined plume of enhanced water vapor situated along the leading edge of the 925 hPa front, similar to that observed in ARs[2] (e.g., Ralph et al. 2004; Bao et al. 2006; Neiman et al. 2008b). This plume intersected the Pacific Northwest from the west at day−1 and from the west–southwest at day0. Core values of IWV exceeded 2.8 cm at both times, although the overall vapor content decreased with time. Companion IVT fields (Figs. 10e,j) depict a plume of strong vapor fluxes whose orientation and position are comparable to the IWV plume. At day −1, the maximum vapor flux within the plume exceeded 600 kg s^{-1} m^{-1} but weakened to 450 kg s^{-1} m^{-1} by day 0. The strong

[2] The compositing approach artificially broadened the width of ARs by nearly a factor of two relative to the width of individual ARs.

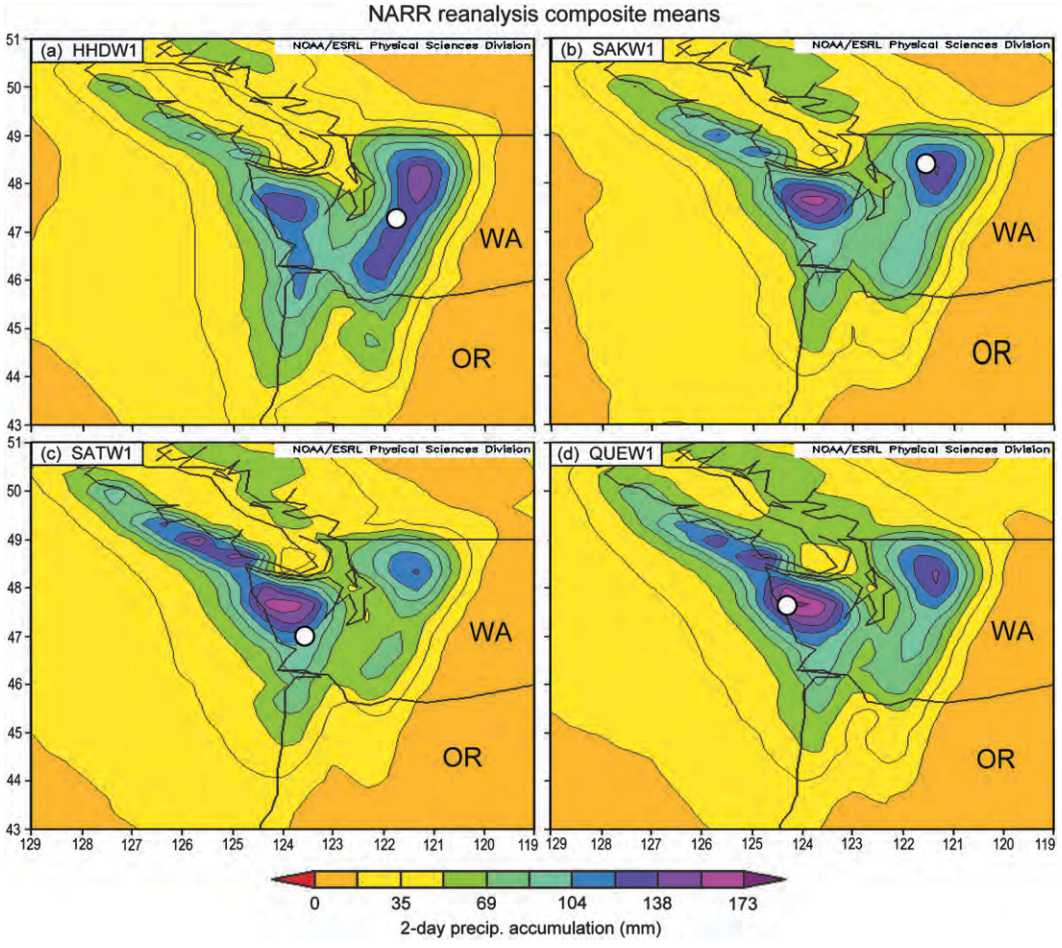

FIG. 9. Composite mean analyses of 2-day precipitation (mm) derived from the NARR daily gridded dataset that combines the day before and the day of the top 10 annual peak daily flows: (a) HHDW1, (b) SAKW1, (c) SATW1, and (d) QUEW1. The white dots show the stream gauge sites.

vapor fluxes within the narrow IWV plume confirm the presence of AR conditions in a composite perspective, and each of the 10 cases that constitute the composite IVT analyses also exhibited filamented AR structure (see supplemental Fig. S1; http://www.ametsoc.org/10.1175/2011JHM1358.s1). The core magnitudes of these composite fluxes (450–600 kg s^{-1} m^{-1}), as well as those in the 10 individual cases [~(500–1300) kg s^{-1} m^{-1}], are representative of those documented during other AR landfalls in the Pacific Northwest (Neiman et al. 2008a,b).

The NARR composite analyses for the top 10 APDFs on the Sauk (Fig. 11), Satsop (Fig. 12), and the Queets (Fig. 13) depict generally similar meteorological conditions as those for the Green APDFs—namely, a trough over the Gulf of Alaska and ridge over California, a frontal baroclinic zone extending offshore from Washington with 4°–6°C anomalies over Washington, and well-defined plumes of IWV and IVT intersecting the Pacific Northwest from offshore. In addition, all IVT analyses from the individual cases on the Sauk, Satsop, and Queets exhibited filamented AR structure (see supplemental Figs. S2–S4; http://www.ametsoc.org/10.1175/2011JHM1358.s1). However, despite these parallels, which would account for generally wet weather across western Washington, significant differences are also apparent. For example, the Queets exhibits, by far, the greatest rise in the melting level between day −1 and day 0 (0.75 km versus 0.2–0.3 km at the three other sites; Fig. 4), thus signifying the strongest warm advection of the four sites. The trough–ridge couplet is least amplified in the Green composites, resulting in low- to midlevel geostrophic flow with nearly zonal orientation (rather than a southwest–northeast orientation) impacting Washington (Figs. 10a,b,f,g). Unlike the Green composites, the Sauk shows 925-hPa cyclogenesis over the Gulf of Alaska,

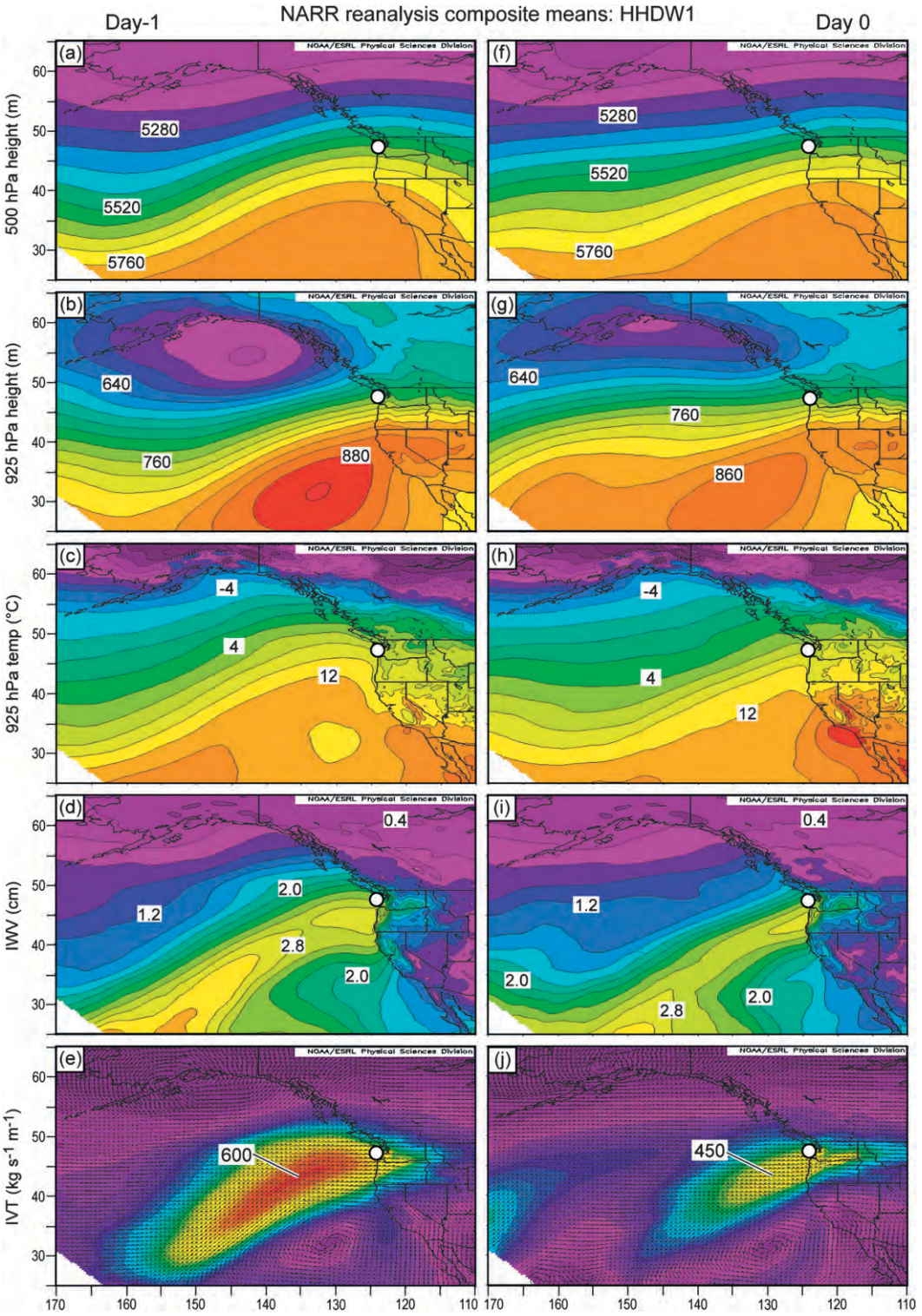

FIG. 10. Composite mean analyses derived from the NARR daily gridded dataset for (a)–(e) the day before and (f)–(j) the day of the top 10 annual peak daily flows at HHDW1: (a),(f) 500 hPa geopotential height (m),(b),(g) 925-hPa geopotential height (m),(c),(h) 925-hPa temperature (°C), (d),(i) IWV (cm), and (e),(j) IVT (kg s^{-1} m^{-1}). The bold white dot in each panel marks the location of the NARR soundings.

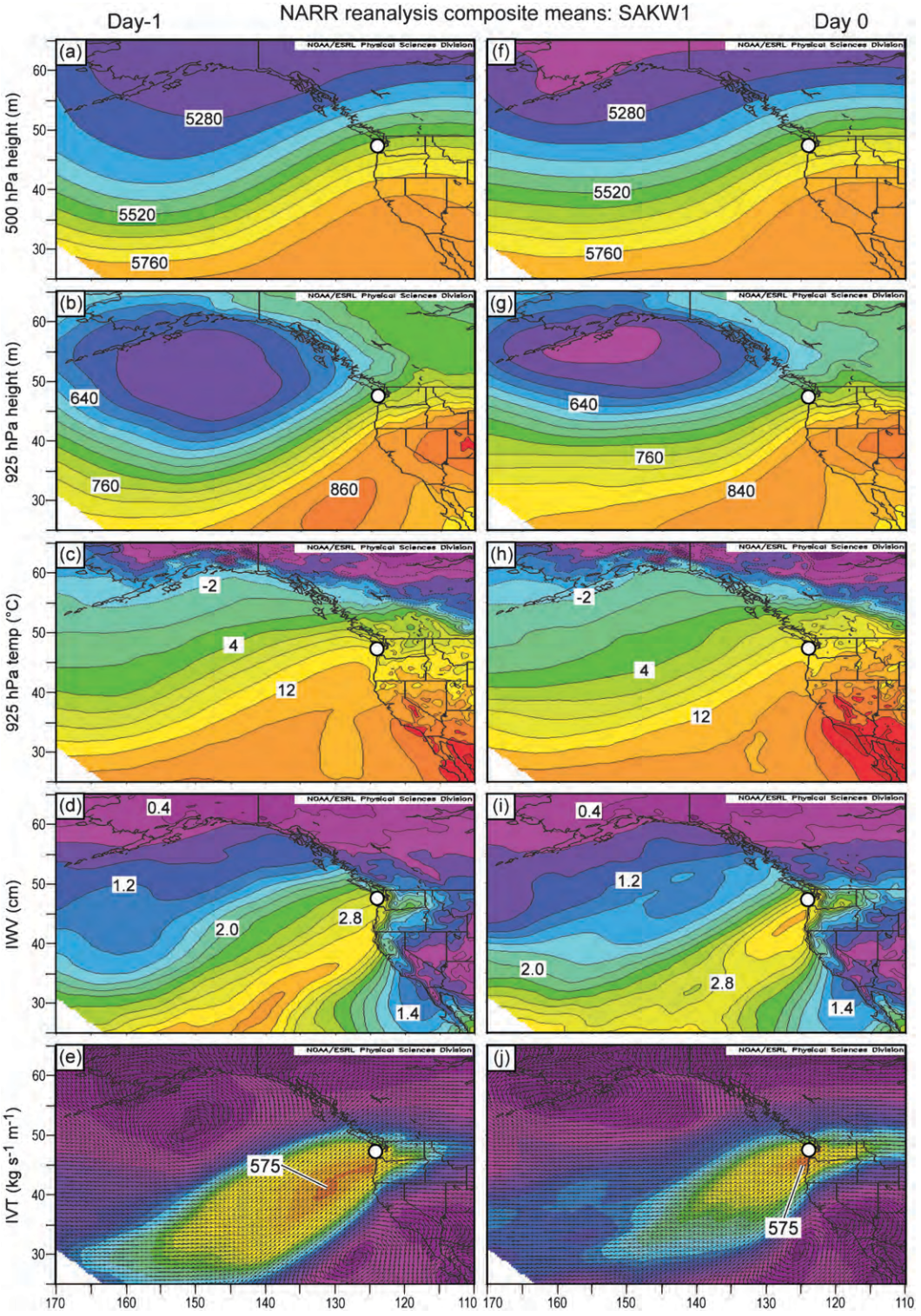

FIG. 11. As in Fig. 10, except for the stream gauge site SAKW1.

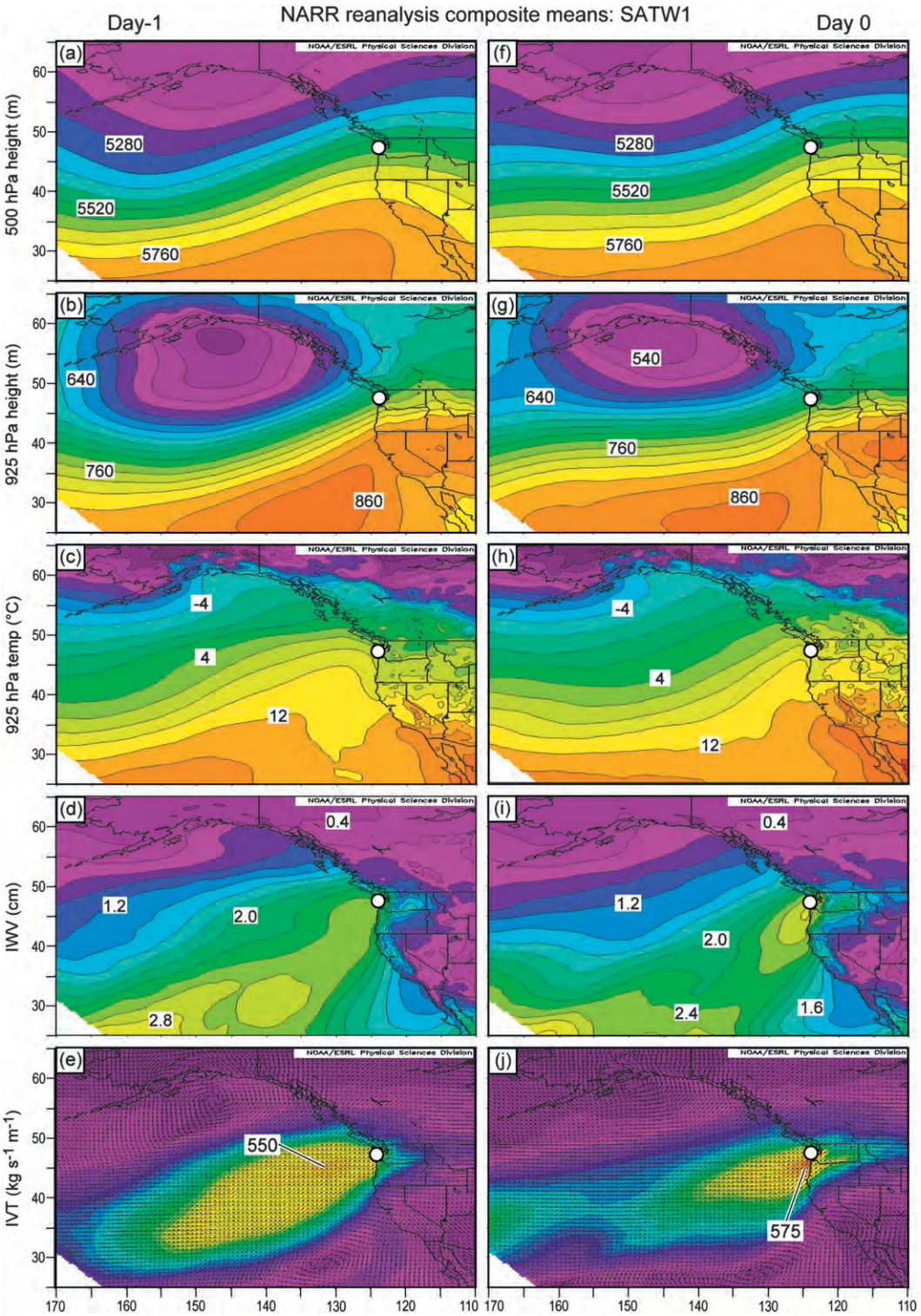

FIG. 12. As in Fig. 10, except for the stream gauge site SATW1.

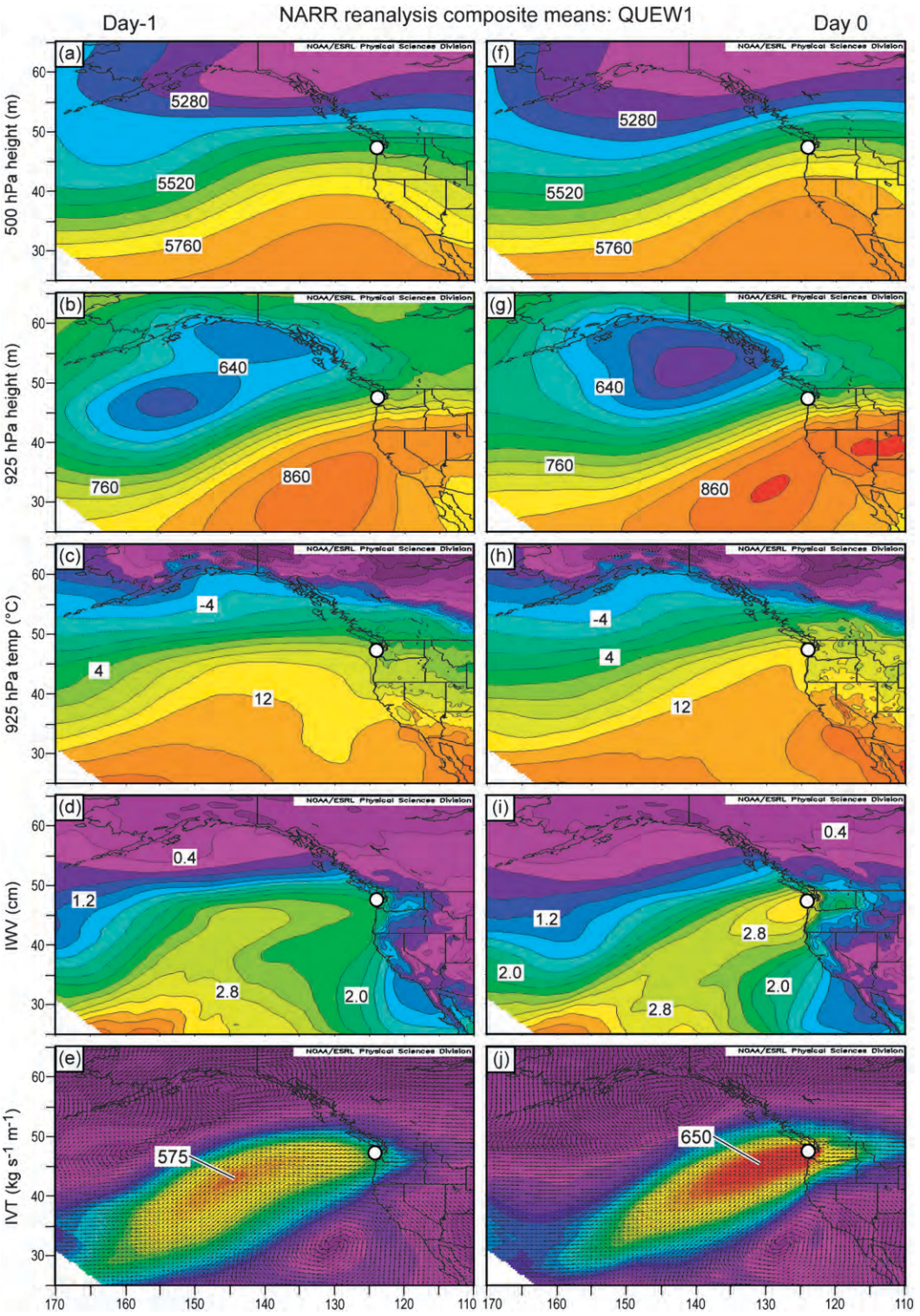

FIG. 13. As in Fig. 10, except for the stream gauge site QUEW1.

with a strong southwesterly fetch into the Pacific Northwest (Figs. 11b,g). The companion IWV plume for the Sauk contains the greatest vapor content of all composite plumes and is the only example clearly depicting a northward advance along the coast (Figs. 11d,i). The Satsop 925-hPa height composites exhibit the strongest low-level cyclone over the Gulf of Alaska (Figs. 12b,g), while the Queets IVT composite at day 0 depicts the strongest AR (exceeding 650 kg s^{-1} m^{-1}) making landfall (Fig. 13j). The Green is the only site of the four where the IVT plume decreases in intensity, rather than maintaining or increasing in strength, during landfall (Figs. 10e,j). The southwest–northeast orientation of the composite AR for the Sauk is similar to that for the Satsop, whereas the Green and Queets composites depict a more zonal orientation of their respective ARs. This key difference is consistent with the fact that the three-dimensional topography of the Pacific Northwest minimally obstructs low-level westerly (southwesterly) flow entering the Green and Queets (Sauk and Satsop) basins, despite the fact that each composite is based on only 10 cases.

The NARR analyses (both individually and the composites) corroborate the results in Fig. 6, which show that landfalling ARs are responsible for nearly all APDFs in western Washington during the 12 most recent water years. In addition, for all peak daily flows that exceeded the 5-yr return period (i.e., the conservative threshold for flooding) on nonconsecutive days in each of the four basins of interest between WY1980 and 2009 (independent of the years they occurred), all corresponding daily IVT analyses from the NARR (not shown) revealed AR conditions. Hence, ARs were responsible for all floods in these basins during the 30-yr period, even though not all ARs during that period generated flooding. Those ARs that produced flooding typically exhibited two or more of the following attributes: (i) the AR was optimally oriented for orographic precipitation enhancement in a given basin, (ii) the low-level onshore water vapor fluxes into the basin were quite strong, (iii) the AR stalled over the basin, (iv) the melting level was especially high, and/or (v) basin soils were already saturated prior to AR landfall. Although the NARR analysis demonstrates that AR orientation and associated low-level flow direction are crucial in dictating which basins are most prone to flooding, the fact that the top 10 APDFs on the Green and Queets, and also on the Sauk and Satsop, share only three dates (or consecutive days) suggest that the other factors listed above can also be important. The composites capture the overall synoptic character and generally vulnerable basins, but they might not always reveal vital details of individual storms and the flood risk to specific basins.

b. Near-shore composite profiles

In an effort to investigate the orographic forcing responsible for the top 10 APFDs at the four sites, daily NARR composite profiles of wind direction, wind speed, equivalent potential temperature (θ_e), and water vapor flux are presented for an offshore grid point close to the Washington coast (46.84°N, 124.42°W) for day −1 and day 0 (Fig. 14); basin-specific surface observations were not used because of the common occurrence of shallow, decoupled stably stratified conditions in western Washington. The NARR composite profiles, which compare favorably with composite profiles generated from operational rawinsonde soundings at Quillayute 120 km to the north (not shown), exhibit several common attributes. For example, strong frictionally induced clockwise turning of wind direction with height occurs in the lowest 1 km (with the lowest wind direction generally from the south–southwest; Figs. 14a,e) in a stably stratified environment (Figs. 14c,g). In addition, a low-level jet resides at ~0.8–1.0 km MSL (especially for the day0 composites) near the top of the shallow directional shear layer (Fig. 14b,f). Companion profiles of relative humidity (not shown) depict nearly saturated conditions (i.e., relative humidities greater than 80%) in the lowest 2.5–5.0 km of the atmosphere. In the 1–2-km MSL layer, weak moist stratification (Figs. 14c,g) occurs in vertical proximity to the strongest incoming water vapor fluxes (Figs. 14d,h). The juxtaposition of the weak stability and strong vapor fluxes yields conditions that are highly conducive to orographic precipitation enhancement, especially given that many catchment basins in western Washington (including the four studied here) extend upward into (or through) this 1–2-km layer. The altitude of maximum water vapor fluxes, just below 1 km MSL and primarily above boundary layer impacts, nearly coincides with the altitude where orographic forcing of precipitation by the upslope flow is statistically most robust in landfalling winter storms impacting California's coastal mountains (based on a multiyear analysis of wind-profiler and GPS data; Neiman et al. 2002, 2009). Above 2 km MSL, clockwise directional shear embedded in strong speed shear and stable stratification reflect conditions associated with warm advection in a baroclinic environment. The directional shear, and hence warm advection, is stronger for day −1.

Despite the similarities in the composite profiles described above, noteworthy differences are also found. Most significantly, the low-level wind direction above the stably stratified near-surface flow is southwesterly for the top 10 APFDs on the Satsop and Sauk, west–southwesterly for the top 10 APDFs on the Queets, and just south of due westerly for the top 10 APDFs on the

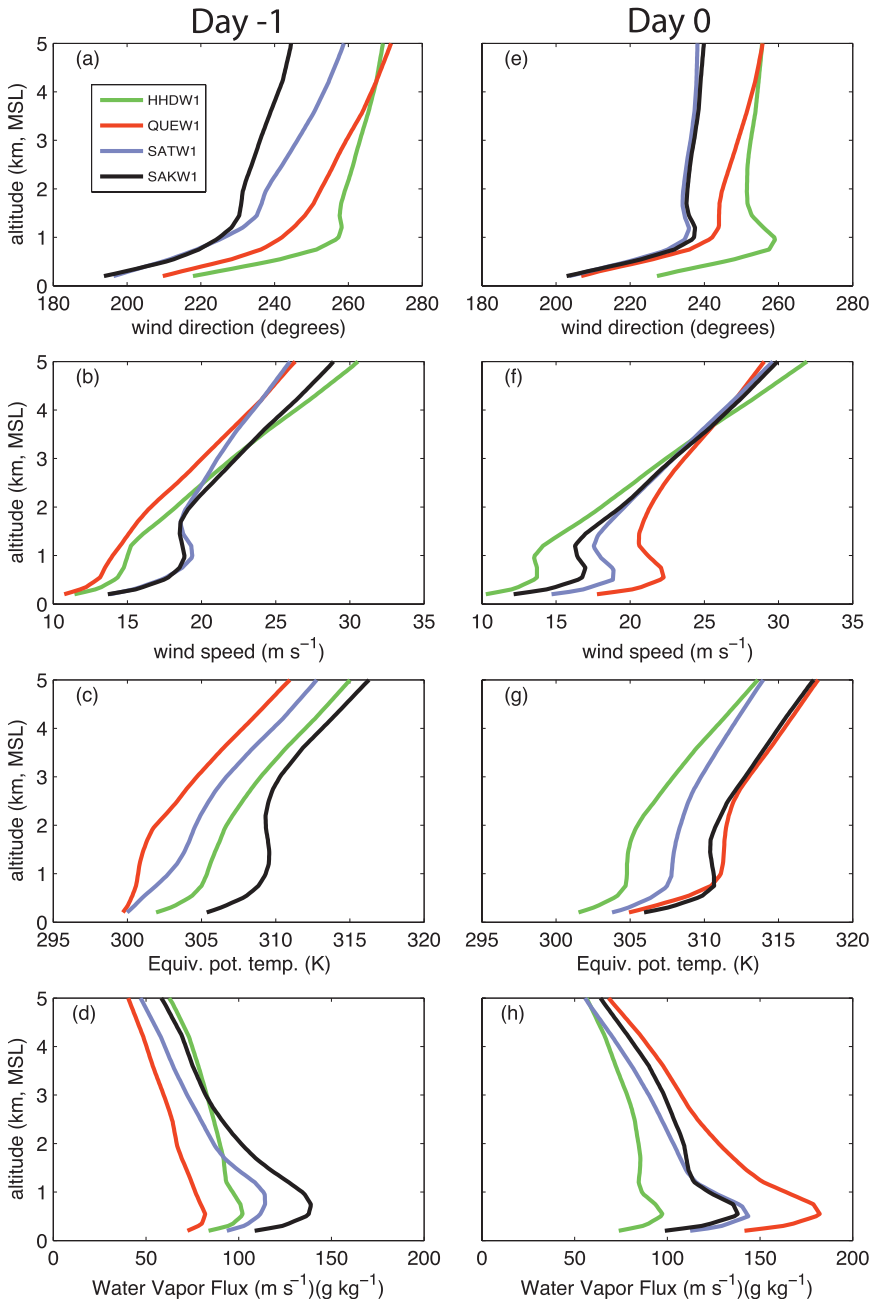

FIG. 14. Composite mean near-offshore profiles from the NARR daily gridded dataset for (a)–(d) the day before and (e)–(h) the day of the top 10 annual peak daily flows at the four stream gauge sites (see color key): (a),(e) wind direction (°), (b),(f) wind speed (m s^{-1}), (c),(g) equivalent potential temperature (K), and (d),(h) total water vapor flux (g kg^{-1} m s^{-1}). The sounding location is shown in Figs. 10–13.

Green (Figs. 14a,e). The reason for these differences, which are also reflected in the 925-hPa composite geopotential height analyses (Figs. 10b,g, 11b,g, 12b,g, 13b,g), becomes apparent upon inspection of the terrain base map in Fig. 3. The Queets basin drains the western flank of the Olympics and optimally intercepts west–southwesterly flow. The Satsop basin on the southern flank of the Olympics optimally intercepts low-level south–southwesterly flow, while the Sauk basin is rain shadowed by the Olympics and the Vancouver Island Mountains for all onshore flow directions other than southwesterly. The upper Green basin is rain shadowed by the Olympics and

Mt. Rainier for all onshore flow directions other than in a narrow window between ~245° and 275°; this window is arguably the most restrictive of the four basins studied here. Results from a one-sided Student's *t* test (not shown) reveal a statistically significant separation (i.e., with >95% confidence) in the basin-averaged low-level wind directions impacting the Green–Queets versus the Sauk–Satsop for the top 10 APDFs. These physically plausible results could also have been modulated by other factors, including the duration and/or strength of AR conditions, water loading, the melting-level altitude, and antecedent soil moisture. Nevertheless, extreme sensitivity of basin runoff to low-level wind direction above the surface has also been observed in the complex topography of coastal California, both during a high-impact landfalling winter storm and from a climatological perspective (Ralph et al. 2003). Specifically, fine details in onshore wind-direction variability there favored major orographic precipitation enhancement with severe flooding in select basins and rain shadowing with modest runoff in adjacent basins.

Additional differences in the NARR composite profiles are evident. Of the four sets of APDFs, the Queets exhibits the greatest increase in θ_e between day −1 and day 0 and the warmest conditions at day 0, whereas the Green experiences slight θ_e cooling during the two-day period and the coldest conditions at day0 (Figs. 14c,g). Because the Green composites possess the weakest meridional component of the four basins, it is not surprising that its mean θ_e is coldest, at least on day 0. The vapor flux profiles (Figs. 14d,h) corroborate the plan-view IVT composites (Figs. 10e,j, 11e,j, 12e,j, 13e,j), including the strongest (weakest) landfalling fluxes occurring at day0 for the Queets (Green) top 10 APDFs. The fact that the top 10 APDFs on the Green occur with the weakest water vapor fluxes and the coldest θ_e values suggests that flooding on the Green is far more sensitive to the flow orientation than to the absolute magnitude of the incoming vapor fluxes, relative to the other basins studied here.

6. Conclusions

This study utilized multiple decades of daily streamflow data gathered along unregulated segments of four major watersheds with uniquely different topographic characteristics in western Washington to determine the meteorological conditions most likely to cause flooding in those watersheds. The Queets and Satsop basins drain the western and southern flanks of the Olympic Mountains, respectively, while the Sauk and Green Rivers flow generally westward from the Cascade Mountains. The Sauk, located in the north Cascades, resides east of the Olympics and the adjacent mountains of Vancouver Island, so direct low-level airflow from the Pacific occurs only from the southwest quadrant. Farther south, the Green is located east–southeast of the Olympics and north of the Mt. Rainier massif. Because of the proximity of these formidable mountains relative to the Green, direct low-level flow from the Pacific occurs only in a narrow wind-direction window from the west–southwest. The basin areas above these four streamflow sites range from 572 to 1848 km^2. Roughly 60% of the Sauk's basin area extends above 1 km MSL, whereas the ~60%–95% of the basin areas in the three other drainages sits below 1 km.

A streamflow analysis was carried out based on the maximum daily flow observed during each water year at each site (i.e., the annual peak daily flow or APDF), with an initial emphasis on the 12 most recent water years between WY1998 and 2009 and then focusing on the 30-year interval between WY1980 and 2009. The shorter time period coincides with relatively complete twice-daily passive microwave satellite coverage of IWV over the Pacific basin. The combination of IWV imagery and streamflow data highlights a close link between landfalling ARs in the Pacific Northwest and APDFs measured at the four sites. Specifically, 46 of the 48 APDFs occurred with landfalling ARs, while the two remaining APDFs were associated with snowmelt. To complement this approach, the three-decade time series of APDFs, which correspond to the availability of the NARR dataset, were examined. The APDFs occurred most often, and were typically largest in magnitude, between November and January. Each site exhibited considerable interannual variability during the 30 years, although the Queets generated the most consistent year-to-year peak flows (i.e., varying by a factor of 3.5) owing to its broad west-facing aspect to the Pacific, whereas the Green displayed the greatest fluctuations (by an order of magnitude) because of the limited onshore wind-direction window (245°–275°) unobstructed by upstream terrain between that watershed and the Pacific.

The NARR was used to assess the composite meteorological conditions associated with the 10 largest APDFs in each of the four watersheds during the 30-year period described above; these conditions are presented schematically in Fig. 15. Significantly, the top 10 APDFs on the Green and Queets Rivers occurred when the mean orientation of landfalling ARs was nearly zonal (Fig. 15a), whereas the top 10 APDFs on the Sauk and Satsop coincided with a mean AR orientation from southwest to northeast (Fig. 15c). This difference yielded contrasting low-level wind-flow fields (i.e., below ~1 km MSL) that optimized the orographic control of precipitation in the relevant watersheds. Specifically, the Queets and Green watersheds experienced their top 10 APDFs when the composite low-level flow was nearly due westerly

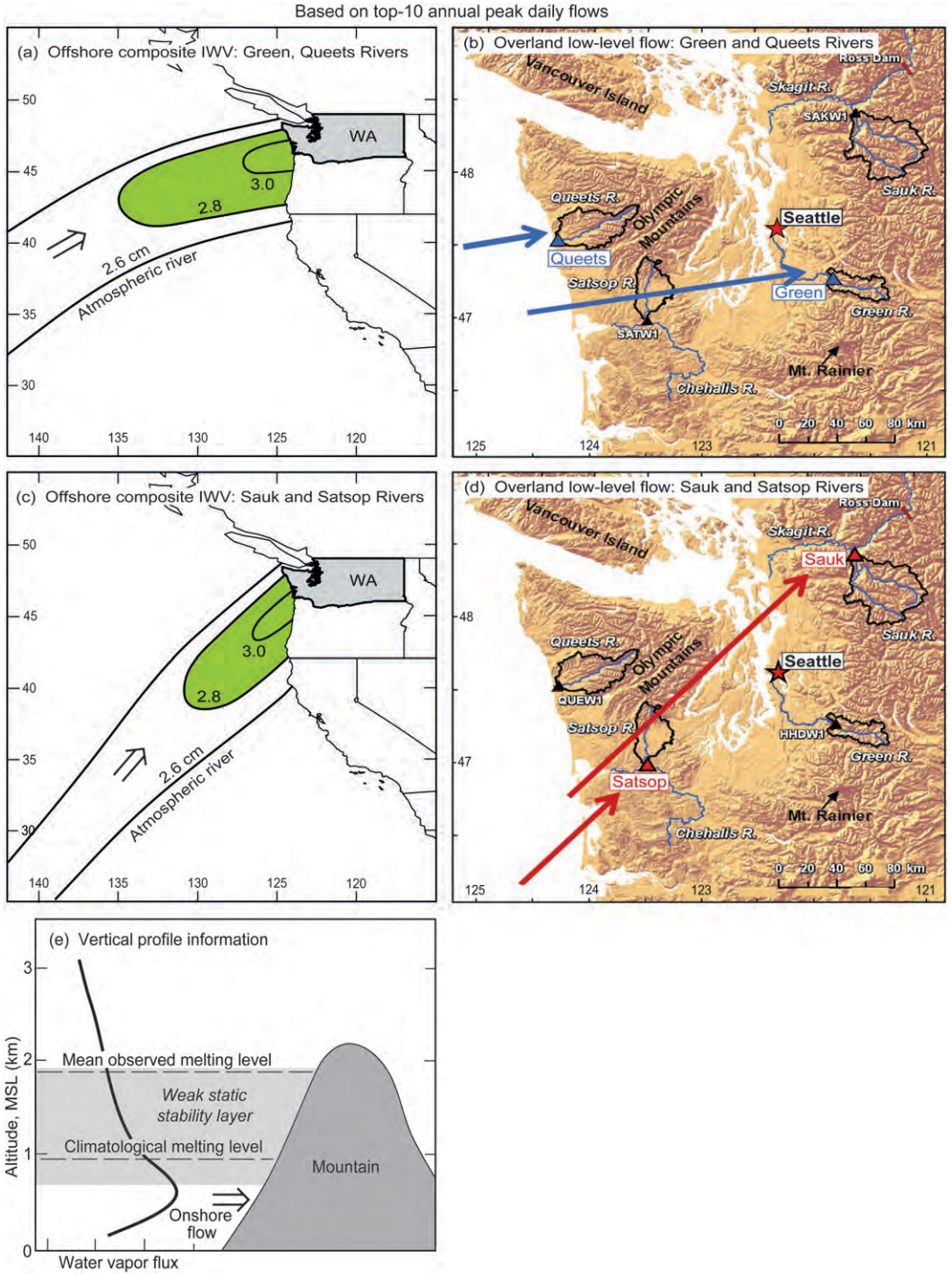

FIG. 15. Conceptual representation of key atmospheric conditions associated with the top 10 annual peak daily flows observed in four watersheds in western Washington. (a) Offshore composite IWV analysis (cm; green shading >2.8 cm) based on the NARR for the Queets and Green Rivers. Washington State is shaded and labeled. (b) Overland composite low-level wind-flow direction (blue arrows) based on the NARR for the Green and Queets Rivers. See Fig. 3 for details on the base map. (c),(d) As in panels (a) and (b), except for the Sauk and Satsop Rivers and red arrows. (e) Composite NARR-based vertical profile information common to all four watersheds in the low-level onshore flow (bold arrow). The upper and lower horizontal dashed lines mark the observed and climatological melting levels, respectively (the climatological melting level is from Minder 2010). Gray shading represents the layer of weak moist static stability. The black curve depicts the water vapor flux profile.

(Fig. 15b), while the Sauk and Satsop had their largest discharges during mean low-level southwesterly flows (Fig. 15d). The disparity in wind direction that generated the largest streamflows highlights the region's complex topography, varied basin orientations, and related rain shadowing relative to the moist low-level airflow in the AR environment.

Despite these differences, the top 10 APDFs on the four watersheds also shared common meteorological attributes (cf. Figs. 9 and 15e). Namely, heavy precipitation fell during the top 10 APDFs, and the composite melting levels estimated from the NARR averaged ~1.9 km MSL, which was anomalously high (by nearly 1 km MSL) and primarily above the four basins of interest. Hence, on average, rain rather than snow fell within almost the entirety of these basins, leading to enhanced runoff. The flooding on the four watersheds occurred during the landfall of ARs within the warm sectors of extratropical cyclones that were accompanied by warm advection, lower-tropospheric temperatures 4°–6°C above normal, strong low-level water vapor fluxes from over the Pacific, and low-level moist-neutral stability. The enhanced onshore vapor fluxes and weak static stability provided a favorable environment for orographic precipitation enhancement across the region's steep terrain. More generally, all peak daily flows that exceeded a 5-yr return period on nonconsecutive days in each of the four basins of interest between WY1980 and 2009 were associated with landfalling ARs.

Further research on establishing linkages between basin characteristics, landfalling ARs, heavy rainfall, and flooding can reveal new knowledge on flood frequencies in storm conditions in the climatologically wet Pacific Northwest. More immediately, knowledge gained from this study can be applied by a host of user communities, including water managers, emergency managers, hydrologists, and weather forecasters. The hydroclimatic linkages established between landfalling ARs and flooding in western Washington can help these (and other) user communities recognize conditions that will lead to flooding in western Washington. For example, enhanced information on potential flooding could be beneficial for dam operations, especially in light of seepage issues incurred at Howard Hanson Dam during the AR of January 2009 (e.g., White et al. 2011). These issues have temporarily reduced flood storage capacity, thus complicating flood-risk management decision making for the heavily populated lower Green River Valley until costly repairs are finalized in the near future. Having improved information to evaluate changing weather and hydrologic forecasts in the context of reservoir storage, basin characteristics, known levee limitations, and other factors can help facilitate these interactions and improve the response to the associated risks. As such, it is our hope that this paper and following studies will allow water managers and other user communities more confidence in making and communicating crucial flood-risk management decisions to their stakeholders and to the public.

Acknowledgments. Cathy Smith and colleagues at NOAA's Earth System Research Laboratory (ESRL) developed the NARR reanalysis composite tools used in this study. Matt Stumbaugh of the U.S. Army Corps of Engineers in Seattle generated the cumulative fraction of basin area graphs using GIS. Kevin Shaffer, also from the Army Corps in Seattle, carried out the recurrence-interval streamflow analysis. Jim Adams assisted in the electronic drafting of figures. We appreciate the comments and suggestions by Drs. Lynn Johnson of NOAA/PSD and Isidora Jankov of NOAA/GSD, and from three anonymous reviewers. Their efforts improved the scope and quality of the manuscript.

REFERENCES

Allan, R. J., J. Lindesay, and D. Parker, 1996: *El Niño, Southern Oscillation and Climate Variability*. CSIRO Publishing, 405 pp.

Bao, J.-W., S. A. Michelson, P. J. Neiman, F. M. Ralph, and J. M. Wilczak, 2006: Interpretation of enhanced integrated water vapor bands associated with extratropical cyclones: Their formation and connection to tropical moisture. *Mon. Wea. Rev.,* **134,** 1063–1080.

Becker, E. J., E. H. Berbery, and R. W. Higgins, 2009: Understanding the characteristics of daily precipitation over the United States using the North American Regional Reanalysis. *J. Climate,* **22,** 6268–6286.

Bukovsky, M. S., and D. J. Karoly, 2007: A brief evaluation of precipitation from the North American Regional Reanalysis. *J. Hydrometeor.,* **8,** 837–846.

Colle, B. A., C. F. Mass, and K. J. Westrick, 2000: MM5 precipitation verification over the Pacific Northwest during the 1997–99 cool seasons. *Wea. Forecasting,* **15,** 730–744.

Daly, C., R. P. Neilson, and D. L. Phillips, 1994: A statistical-topographic model for mapping climatological precipitation over mountainous terrain. *J. Appl. Meteor.,* **33,** 140–158.

Dettinger, M. D., 2004: Fifty-two years of "pineapple-express" storms across the west coast of North America. California Climate Change Center Rep. Series 2005-003, 15 pp. [Available online at http://www.energy.ca.gov/2005publications/CEC-500-2005-004/CEC-500-2005-004.PDF.]

Hollinger, J. P., J. L. Peirce, and G. A. Poe, 1990: SSM/I instrument evaluation. *IEEE Trans. Geosci. Remote Sens.,* **28,** 781–790.

Kalnay, E., and Coauthors, 1996: The NCEP/NCAR 40-Year Reanalysis Project. *Bull. Amer. Meteor. Soc.,* **77,** 437–471.

Knippertz, P., and H. Wernli, 2010: A Lagrangian climatology of tropical moisture exports to the Northern Hemispheric extratropics. *J. Climate,* **23,** 987–1003.

Lackmann, G. M., and J. R. Gyakum, 1999: Heavy cold-season precipitation in the northwestern United States: Synoptic climatology and an analysis of the flood of 17–18 January 1986. *Wea. Forecasting,* **14,** 687–700.

Lundquist, J. D., P. J. Neiman, B. E. Martner, A. B. White, D. J. Gottas, and F. M. Ralph, 2008: Rain versus snow in the Sierra Nevada, California: Comparing Doppler profiling radar and surface observations of melting level. *J. Hydrometeor.,* **9,** 194–211.

Madden, R., and P. Julian, 1994: Observations of the 40–50 day tropical oscillation—A review. *Mon. Wea. Rev.,* **122,** 814–837.

Mantua, N. J., S. R. Hare, Y. Zhang, J. M. Wallace, and R. C. Francis, 1997: A Pacific interdecadal climate oscillation with impacts on salmon production. *Bull. Amer. Meteor. Soc.,* **78,** 1069–1079.

Mastin, M. C., A. S. Gendaszek, and C. R. Barnas, 2010: Magnitude and extent of flooding at selected river reaches in western Washington, January 2009. U.S. Geological Survey Scientific Investigations Rep. 2010-5177, 34 pp.

Mesinger, F., and Coauthors, 2006: North American Regional Reanalysis. *Bull. Amer. Meteor. Soc.,* **87,** 343–360.

Milly, P. C. D., J. Betancourt, M. Falkenmark, R. M. Hirsch, Z. W. Kundzewicz, D. P. Lettenmaier, and R. J. Stouffer, 2008: Stationarity is dead: Wither water management? *Science,* **319,** 573–574.

Minder, J. R., 2010: The sensitivity of mountain snowpack accumulation to climate warming. *J. Climate,* **23,** 2634–2650.

——, D. R. Durran, G. H. Roe, and A. M. Anders, 2008: The climatology of small-scale orographic precipitation over the Olympic Mountains: Patterns and processes. *Quart. J. Roy. Meteor. Soc.,* **134,** 817–839.

Mo, K. C., M. Chelliah, M. L. Carrera, R. W. Higgins, and W. Ebisuzaki, 2005: Atmospheric moisture transport over the United States and Mexico as evaluated in the NCEP Regional Reanalysis. *J. Hydrometeor.,* **6,** 710–728.

Neiman, P. J., F. M. Ralph, A. B. White, D. E. Kingsmill, and P. O. G. Persson, 2002: The statistical relationship between upslope flow and rainfall in California's coastal mountains: Observations during CALJET. *Mon. Wea. Rev.,* **130,** 1468–1492.

——, ——, G. A. Wick, Y.-H. Kuo, T.-K. Wee, Z. Ma, G. H. Taylor, and M. D. Dettinger, 2008a: Diagnosis of an intense atmospheric river impacting the Pacific Northwest: Storm summary and offshore vertical structure observed with COSMIC satellite retrievals. *Mon. Wea. Rev.,* **136,** 4398–4420.

——, ——, ——, J. Lundquist, and M. D. Dettinger, 2008b: Meteorological characteristics and overland precipitation impacts of atmospheric rivers affecting the West Coast of North America based on eight years of SSM/I satellite observations. *J. Hydrometeor.,* **9,** 22–47.

——, A. B. White, F. M. Ralph, D. J. Gottas, and S. I. Gutman, 2009: A water vapour flux tool for precipitation forecasting. *Water Manage.,* **162,** 83–94.

Ralph, F. M., P. J. Neiman, D. E. Kingsmill, P. O. G. Persson, A. B. White, E. T. Strem, E. D. Andrews, and R. C. Antweiler, 2003: The impact of a prominent rain shadow on flooding in California's Santa Cruz Mountains: A CALJET case study and sensitivity to the ENSO cycle. *J. Hydrometeor.,* **4,** 1243–1264.

——, ——, and G. A. Wick, 2004: Satellite and CALJET aircraft observations of atmospheric rivers over the eastern North Pacific Ocean during the winter of 1997/98. *Mon. Wea. Rev.,* **132,** 1721–1745.

——, ——, and R. Rotunno, 2005: Dropsonde observations in low-level jets over the northeastern Pacific Ocean from CALJET-1998 and PACJET-2001: Mean vertical-profile and atmospheric-river characteristics. *Mon. Wea. Rev.,* **133,** 889–910.

——, ——, G. A. Wick, S. I. Gutman, M. D. Dettinger, D. R. Cayan, and A. B. White, 2006: Flooding on California's Russian River: The role of atmospheric rivers. *Geophys. Res. Lett.,* **33,** L13801, doi:10.1029/2006GL026689.

——, ——, G. N. Kiladis, K. Weickmann, and D. W. Reynolds, 2011: A multiscale observational case study of a Pacific atmospheric river exhibiting tropical–extratropical connections and a mesoscale frontal wave. *Mon. Wea. Rev.,* **139,** 1169–1189.

Rogers, E., cited 2005: On-line documentation of mesoscale branch model changes. [Available online at www.emc.ncep.noaa.gov/mmb/mmbpll/eric.html#TAB4.]

Ruane, A. C., 2010: NARR's atmospheric water cycle components. Part I: 20-year mean and annual interactions. *J. Hydrometeor.,* **11,** 1205–1219.

Schluessel, P., and W. J. Emery, 1990: Atmospheric water vapour over oceans from SSM/I measurements. *Int. J. Remote Sens.,* **11,** 753–766.

Steenburgh, W. J., C. F. Mass, and S. A. Ferguson, 1997: The influence of terrain-induced circulations on wintertime temperature and snow level in the Washington Cascades. *Wea. Forecasting,* **12,** 208–227.

Stewart, R. E., J. D. Marwitz, J. C. Pace, and R. E. Carbone, 1984: Characteristics through the melting layer of stratiform clouds. *J. Atmos. Sci.,* **41,** 3227–3237.

Stohl, A., C. Forster, and H. Sodemann, 2008: Remote sources of water vapor forming precipitation on the Norwegian west coast at 60°N—A tale of hurricanes and an atmospheric river. *J. Geophys. Res.,* **113,** D05102, doi:10.1029/2007JD009006.

USGS, 1981: Guidelines for determining flood flow frequency. Hydrology Subcommittee Bulletin 17B, 188 pp. [Available from U.S. Department of the Interior, Geological Survey, Office of Water Data Coordination, 417 National Center, Reston, VA 22092.]

Wentz, F. J., 1995: The intercomparison of 53 SSM/I water vapor algorithms. Remote Sensing Systems Tech. Rep. on WetNet Water Vapor Intercomparison Project (VIP), 19 pp.

West, G. L., W. J. Steenburgh, and W. Y. Y. Cheng, 2007: Spurious grid-scale precipitation in the North American Regional Reanalysis. *Mon. Wea. Rev.,* **135,** 2168–2184.

White, A. B., D. J. Gottas, E. Strem, F. M. Ralph, and P. J. Neiman, 2002: An automated bright-band height detection algorithm for use with Doppler radar vertical spectral moments. *J. Atmos. Oceanic Technol.,* **19,** 687–697.

——, and Coauthors, 2011: NOAA's rapid response to the Howard A. Hanson Dam flood risk management crisis. *Bull. Amer. Meteor. Soc.,* in press.

Zhu, Y., and R. E. Newell, 1998: A proposed algorithm for moisture fluxes from atmospheric rivers. *Mon. Wea. Rev.,* **126,** 725–735.